232045

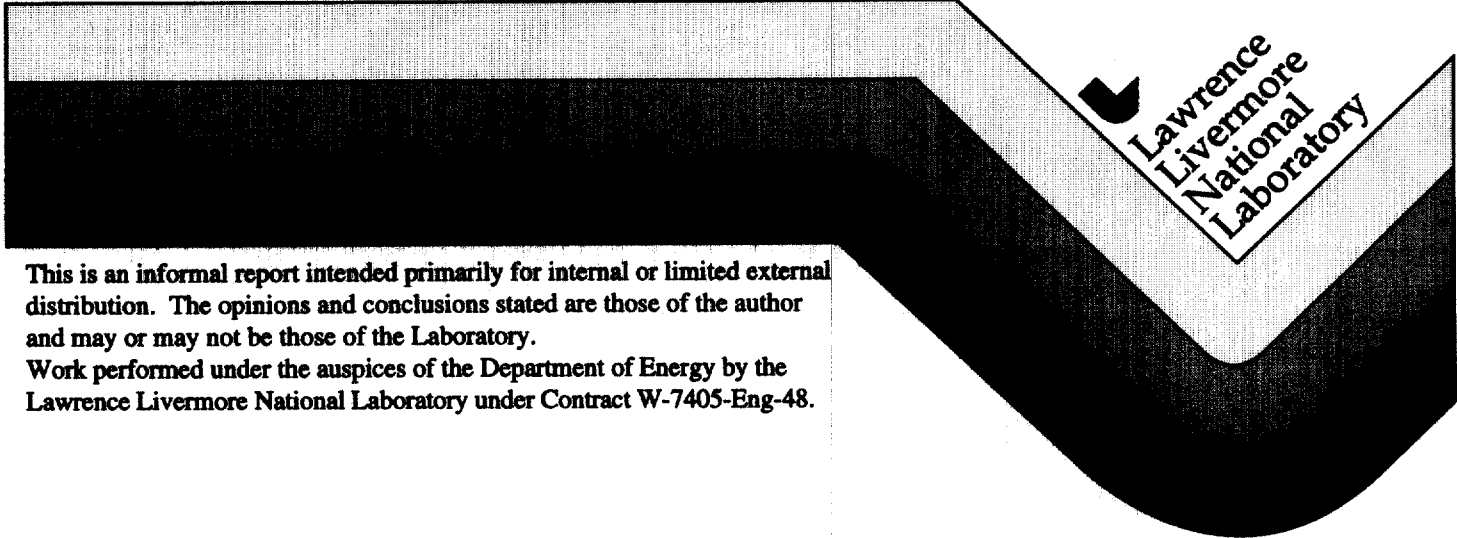# Modeling Electron Heat Transport During Magnetic Field Buildup in SSPX

D. D. Hua, E. B. Hooper, T. K. Fowler

October, 1997

Lawrence Livermore National Laboratory

D. D. Hua, E. B. Hooper, T. K. Fowler

October, 1997

Lawrence
Livermore
National
Laboratory

Modeling Electron Heat Transport During Magnetic Field Buildup in SSPX

D. D. Hua,[a] E. B. Hooper[b] and T. K. Fowler[a]

[a]Department of Nuclear Engineering
University of California
Berkeley, CA 94720

[b]Lawrence Livermore National Laboratory
University of California
Livermore, CA 94551

Abstract

A model for spheromak magnetic field buildup and electron thermal transport, including a thermal diffusivity associated with magnetic turbulence during helicity injection [1], is applied to a SSPX equilibrium, with a maximum final magnetic field of 1.3 T. Magnetic field-buildup times of 1.0×10^{-3}, 5.0×10^{-4} and 1.0×10^{-4} s were used in the model to examine their effects on electron thermal transport. It is found that at transport run time of 4×10^{-3} s, the fastest buildup-time results in the highest final temperature profile, with a core temperature of 0.93 keV while requiring the lowest input energy at 140 KJ. The results show that within the model the most rapid buildup rate generates the highest electron temperature at the fastest rate and at the lowest consumption of energy. However, the peak power requirements are large (> 600 MW for the fastest buildup case examined), suggesting that effects such as impurity generation, which lie outside the model, may lead to a rate which

1 Introduction

The following model, in *cylindrical coordinates* and calibrated to CTX [1], is applied to the SSPX,

$$\frac{\partial}{\partial t}\left[\frac{3}{2}nT\right] + \frac{1}{r}\frac{\partial}{\partial r}\left[rn\chi\left(\frac{\partial T}{\partial r}\right)\right] = \eta j^2 \qquad (1)$$

$$\frac{\partial}{\partial t}\left[\frac{B^2}{2\mu}\right] + \frac{1}{r}\frac{\partial}{\partial r}\left[rP(r)\right] = -\eta j^2 , \qquad (2)$$

where Eq. (1) is the temperature diffusion equation and Eq. (2) the magnetic energy diffusion equation. Here all quantities are expressed in MKS units except for T, which is in keV. In the equations, $n(r)$ is the electron density (in units of 10^{20} m^{-3}), $T(r,t)$ the electron temperature, $B(r,t)$ the magnetic field, and $P(r) = \pm(v_A \tilde{B}^2/\mu)$ the Poynting vector (representing helicity injection that drives the turbulent magnetic field $\tilde{B}$) where $v_A = 1.63 \times 10^6 (B/\sqrt{n})$ $[m/s]$ is the Alfvén speed. In addition, ηj^2 is the Ohmic heating where $\eta = (4 \times 10^{-8})T^{-\frac{3}{2}}$ $[W/(m^3 A^2)]$ is the Spitzer resistivity and $j = (\lambda B/\mu)$ is the current density, obtained from Maxwell's equations and the Taylor state [2], assumed in this model. The diffusion coefficient in Eq. (1) is

$$\chi = \chi_{GB} + \chi_{mag}$$

where

$$\chi_{GB} = \left[\frac{0.6T^{\frac{3}{2}}}{B^2 a}\right] , \qquad (3)$$

$$\chi_{mag} = v_e L_c \left[\frac{\tilde{B}}{B}\right]^2 . \qquad (4)$$

χ_{GB} is an approximate Gyrobohm diffusion coefficient arising from electrostatic turbulence, and χ_{mag} is the Rechester-Rosenbluth coefficient arising from magnetic turbulence [3]. In Eqs. (3) and (4) a is the minor radius, $v_e = 1.88 \times 10^7 \sqrt{T}$ $[m/s]$ the electron thermal speed, and $L_c = 3.2a$ from fitting previous results to CTX data [1, 4]. Manipulating Eq. (2) to get $\tilde{B}$ in terms of other quantities [1],[1] we arrive at

---

[1] we have modeled the spheromak as a cylinder with length ($2\pi a$) and radius a.

$$\chi_{mag} = \frac{v_e L_c \mu}{v_A B^2} \left[\frac{P_\Omega(r)}{(2\pi)^2 ar} \right] g_p(r) \qquad (5)$$

where

$$P_\Omega(r) = \int^r dV \, \eta j^2$$

$$g_p(r) = \left| \left[\frac{\int^r dV B^2}{\int^a dV B^2} \right] \frac{\int^a dV \frac{\partial}{\partial t} \left[\frac{B^2}{2\mu} \right]}{P_\Omega(r)} + 1 \right| = \left| \left[\frac{\int^r dV B^2}{\int^a dV B^2} \right] \frac{P_m}{P_\Omega(r)} + 1 \right| . \qquad (6)$$

In Eq. (6), $P_\Omega(r)$ is the partial Ohmic power ($P_\Omega(a)$ is the total Ohmic power. For the rest of this paper, P_Ω means the total Ohmic power) and $P_m \equiv \int^a dV \frac{\partial}{\partial t} \left[\frac{B^2}{2\mu} \right]$ is the magnetic power, defined as that part of the input power spent in building up the magnetic field. Hence $[g_p(a) - 1]$ is the ratio of magnetic power to Ohmic power. As explained in Ref. [1], Eqs. (5) and (6) are derived by integrating Eq. (2) in r assuming $B(r)$ is of constant shape representative of the Taylor state and using this to derive $\tilde{B}^2$ appearing in χ_{mag}. It is this procedure that gives rise to the form factor appearing in Eq. (6).

2   Corsica Results for SSPX

The diffusion coefficients defined in Eqs. (3) and (5) are substituted into the transport module of *corsica* [5], a general plasma equilibrium and transport code written in flux variables with effective minor radius $\bar{\rho}$ given by

$$\bar{\rho} = \frac{\psi}{\psi_{max}}$$

with ψ being the *toroidal* flux coordinate. In addition, the magnetic field $B(\bar{\rho}, t) \equiv \sqrt{\langle B^2 \rangle}$ where $\langle \cdot \rangle$ represents the flux surface average. To utilize our model described in Section 1 in *corsica*, the integration limits in Eq. (6) become $\bar{\rho}$ and in the denominator of Eq. (5) we set $r = a\bar{\rho}^{\frac{1}{2}}$, representative of the behavior of ψ near the origin.

The prescribed magnetic field and its time-derivative are

$$B(\bar{\rho}, t) = B_i(\bar{\rho}) + [B_f(\bar{\rho}) - B_i(\bar{\rho})] \left(1 - e^{-\frac{t}{\tau}} \right) \qquad (7)$$
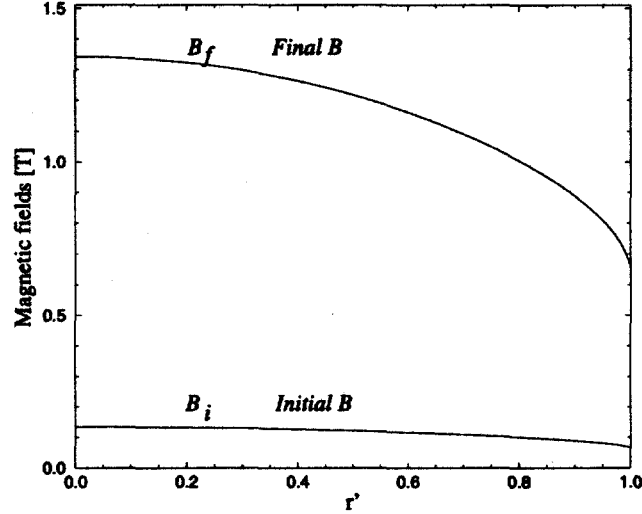
3

Figure 1: Initial and final magnetic field profiles.

$$\dot{B}(\bar{\rho}, t) \;=\; \frac{1}{\tau} \left[B_f(\bar{\rho}) - B_i(\bar{\rho}) \right] e^{-\frac{t}{\tau}} \; . \tag{8}$$

where $B_i(\bar{\rho})$ is the initial field and has an arithmetic mean of 0.1 T and $B_f(\bar{\rho})$ is the final field and has a mean of 1.0 T. $B_i(\bar{\rho})$ and $B_f(\bar{\rho})$, by construction, have the same spatial profile. Fig. 1 plots B_i and B_f versus r', defined as

$$r' = \bar{\rho}^{\frac{1}{2}} \; .$$

In all subsequent figures, spatial profiles are plotted in the r' variable. In Eqs. (7) and (8), τ is the characteristic field buildup time. The following buildup times, $\tau_1 = 1.0 \times 10^{-3}$, $\tau_2 = 5.0 \times 10^{-4}$ and $\tau_3 = 1.0 \times 10^{-4}$ s are used in the corsica runs. The transport run time is set to 4.0×10^{-3} s, approximately the proposed SSPX magnetic gun time.

The initial temperature profile is $T_i(\bar{\rho}) = 0.02$ keV, a flat profile, and the boundary condition is $T(\bar{\rho} = 1) = 0.02$ keV.[2] Also, the density and q profiles, plotted in Fig. 2, are kept constant during the transport run.

The time-evolution of the thermal diffusivities, temperature, energy and other quantities

---

[2]The other boundary condition, $\frac{dT}{dr}\big|_{r=0} = 0$ is automatically satisfied if $\frac{dT}{d\bar{\rho}}\big|_{\bar{\rho}=0}$ is finite.
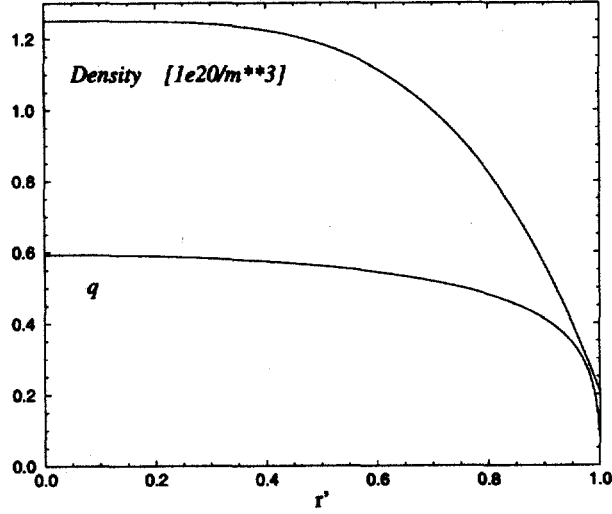
4

Figure 2: q and density profile of a SSPX equilibrium.

of interest are presented in the following sections. For convenience, quantities associated with τ_1, τ_2 and τ_3 will be subscripted 1, 2 and 3 respectively.

2.1 Thermal Diffusivity

Fig. 3 plots the initial and final χ profiles for τ_1, τ_2 and τ_3. The initial temperature, at 0.02 keV, is low, thus χ_{GB} is much smaller than χ_{mag} and could be ignored, except at $r' = 0$ where $\chi_{mag} = 0$. Initially, χ_{mag} is quite high due to a big $\dot{B}$ in Eq. (8) which leads to a big g_p in Eq. (6) which then leads to a big χ_{mag} in Eq. (5). The initial $\dot{B}$'s also cause χ_3 to be an order of magnitude bigger than χ_1: since $\tau_3 \ll \tau_1$, then $\dot{B}_3 \gg \dot{B}_1$ from Eq. (8), which leads to $P_{m3} \gg P_{m1}$, and since $P_{\Omega 3} = P_{\Omega 1}$, then $g_{p3} \gg g_{p1}$ from Eq. (6) ($\gg$ here means approximately an order of magnitude bigger).

The situation reverses at $t = 4.0 \times 10^{-3}$ s where $\dot{B}$ becomes small as prescribed by Eq. (8) which lowers g_p and thus χ_{mag}. In fact, $\dot{B}_3 \approx 0$ leads to $g_{p3} \approx 1$. In contrast, $\dot{B}_1 \not\approx 0$ so that $P_{m1} \approx P_{\Omega 1}$ (see Fig. 4) which leads to $g_{p1} > 1$. Therefore $g_{p3} < g_{p1}$ and is the main reason that $\chi_{mag3} < \chi_{mag1}$.

Continuing with Fig. 3, near $r' = 0$ where $\chi_{mag} \to 0$ and temperature is highest, $\chi_{GB} \geq \chi_{mag}$ and becomes significant. Since the temperature profile for τ_3 is higher than
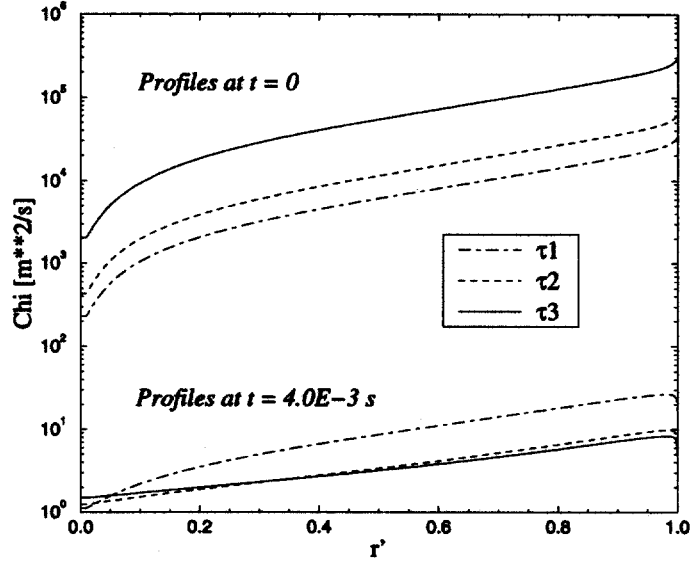
5

Figure 3: Initial and final χ profiles for field buildup times τ_1, τ_2 and τ_3.

the profile for τ_1 (see Fig. 6), then $\chi_{GB3} > \chi_{GB1}$. Therefore, for $0 < r' < 0.05$, $\chi_3 > \chi_1$ due to $\chi_{GB3} > \chi_{GB1}$ and χ_{mag} being small, and for $0.05 < r' < 1$, $\chi_3 < \chi_1$ due to $\chi_{mag3} < \chi_{mag1}$ and χ_{GB} being small.

Fig. 4 plots the time-evolution of magnetic powers P_m and Ohmic powers P_Ω. From Fig. 4, P_{m3} and $P_{\Omega3}$ peak higher and earlier than P_{m2} and $P_{\Omega2}$ respectively, which peak higher and earlier than P_{m1} and $P_{\Omega1}$ respectively. However, P_{m3} and $P_{\Omega3}$ also decrease faster than P_{m2} and $P_{\Omega2}$ respectively which also in turn decrease faster than P_{m1} and $P_{\Omega1}$.

The relative behavior of P_{m3} and P_{m2} is due to a more rapid build up and maintenance of the magnetic field for buildup time τ_3 than τ_2, where $B_3 > B_2$ and $\dot{B}_3 > \dot{B}_2$ in the beginning, but $B_3 > B_2$ and $\dot{B}_3 \ll \dot{B}_2$ after some elapsed time. Similarly, B_2, B_1, $\dot{B}_2$ and $\dot{B}_1$ follow the same trend to affect the relative behavior of P_{m2} and P_{m1}. The relative behavior of P_Ω's is due to $B_3 > B_2 > B_1$ combined with the opposite effect of $T_3 > T_2 > T_1$ (see Section 2.2).

Also from Fig. 4, $P_{m3} < P_{\Omega3}$ for $t > 6 \times 10^{-4}$ s and rapidly approaches 0. Similarly, $P_{m2} < P_{\Omega2}$ for $t > 2.4 \times 10^{-3}$ s and approaches 0. In contrast, $P_{m1} \approx P_{\Omega1}$ at the final time $t = 4.0 \times 10^{-3}$ s. The evolution of the ratio of P_m to P_Ω plays a significant role in determining the effectiveness of input energy in heating the plasma (see Sect. 2.3).
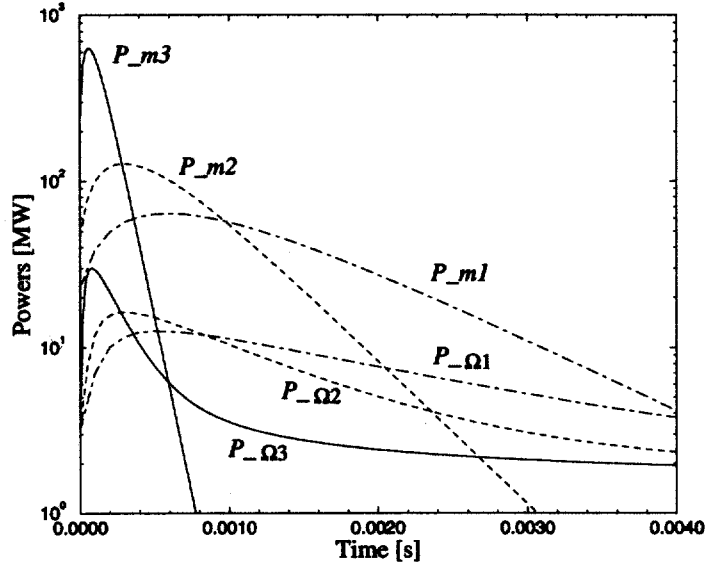
6

Figure 4: Time evolution of magnetic power P_m and Ohmic power P_Ω for buildup times τ_1, τ_2 and τ_3.

Defining the average χ as $\bar{\chi} = (\int dV \, \chi)/V$, Fig. 5 plots the time-evolution of $\bar{\chi}$ for τ_1, τ_2 and τ_3. With trends similar to those in Fig. 3, $\bar{\chi}_3 > \bar{\chi}_2 > \bar{\chi}_1$ initially. But $\bar{\chi}_3 < \bar{\chi}_1$ for $t > 5 \times 10^{-5}$ s and $\bar{\chi}_3 < \bar{\chi}_2$ for $t > 3.4 \times 10^{-5}$ s, while $\bar{\chi}_2 < \bar{\chi}_1$ for $t > 9 \times 10^{-5}$ s.

2.2 Temperature

Fig. 6 plots the final temperature profiles for buildup times τ_1, τ_2 and τ_3 (initial profiles are the same, all at a uniform 0.02 keV). The respective core temperatures are $T_{c1} = 0.62$ keV, $T_{c2} = 0.81$ keV and $T_{c3} = 0.93$ keV. Fig. 7 plots the respective normalized temperature profiles. While the profiles for τ_2 and τ_3 are similar, they are both flatter than that for τ_1. The similarity of the profile for the two faster buildup rates indicates that it has reached a final shape; profile evolution is continuing for the slowest rate.

Fig. 8 plots the time evolution of the respective core temperatures, $T(r' = 0)$. As expected from Figs. 4 and 5, T_{c3} rises faster than T_{c2} which in turn rises faster than T_{c1} in the beginning due to $P_{\Omega3} > P_{\Omega2} > P_{\Omega1}$ and $\bar{\chi}_3 < \bar{\chi}_2 < \bar{\chi}_1$ (for $t > 5 \times 10^{-5}$ s). However near $t = 4.0 \times 10^{-3}$ s, T_{c3} rises slower than T_{c2} which rises slower than T_{c1}, because of
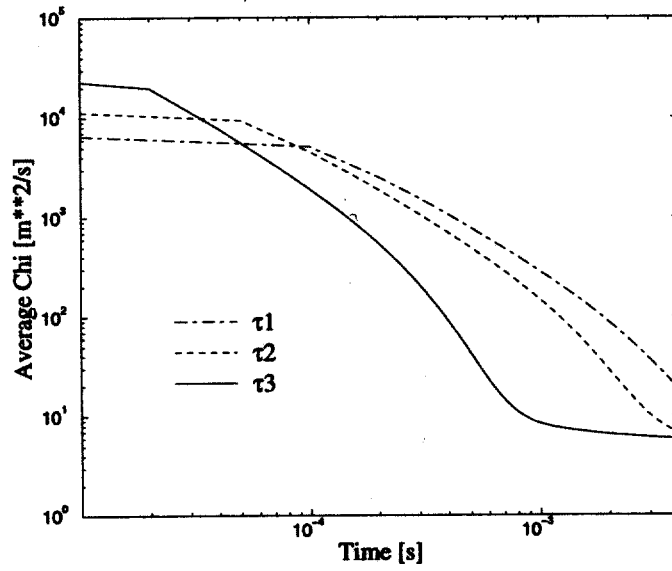
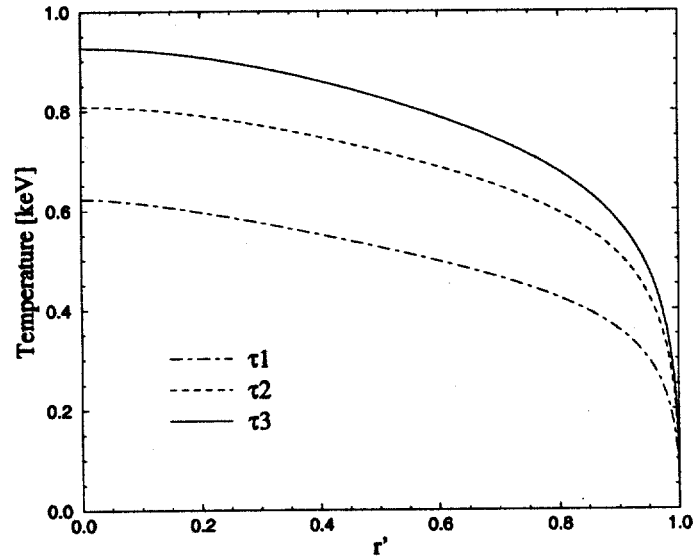Figure 5: Time evolution of the $\bar{\chi}$ for buildup times τ_1, τ_2 and τ_3.

Figure 6: Final temperature profiles for buildup times τ_1, τ_2 and τ_3.
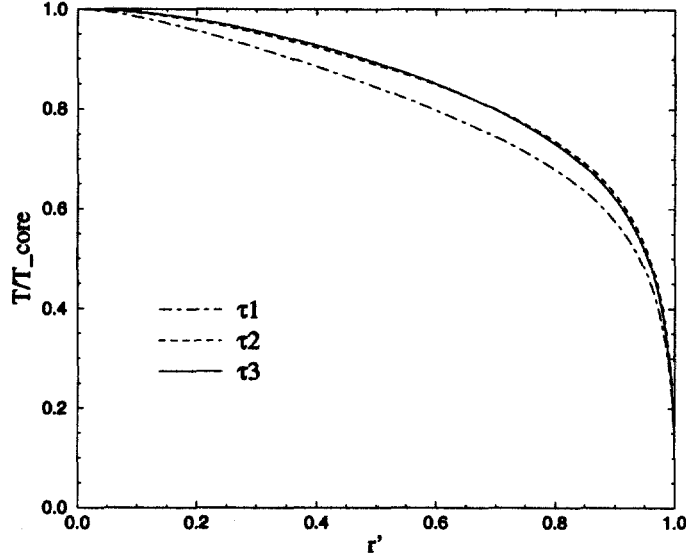
Figure 7: Normalized final temperature profiles for buildup times τ_1, τ_2 and τ_3.

$P_{\Omega 3} < P_{\Omega 2} < P_{\Omega 1}$ despite $\bar{\chi}_3 < \bar{\chi}_2 < \bar{\chi}_1$. Within this model, we have not reached an equilibrium, steady state temperature, even for the fastest buildup rate examined.

2.3 Energy

Fig. 9 plots the time evolution of the input energy, defined as

$$E_{in} = \int dt \; [P_m + P_\Omega]$$

for buildup times τ_1, τ_2 and τ_3. As expect from Fig. 4, E_{in3} rises faster and becomes nearly flat sooner than E_{in2}, which retains the same trends with respect to E_{in1}. It is interesting to note that $E_{in3} < E_{in2} \approx E_{in1}$ at $t = 4 \times 10^{-3}$ s. This is due to $(P_{m3}, P_{\Omega 3}) < (P_{m2}, P_{\Omega 2})$ and $(P_{m1}, P_{\Omega 1})$ respectively for $t > 6 \times 10^{-4}$ s from Fig. 4, as explained in Section 2.1.

It is also of interest to determine the effectiveness of the input energy in heating the plasma. Fig. 10 plots T_c versus E_{in}. It takes 150 KJ to get a core temperature of 0.62 keV for buildup time τ_1, and 150 KJ to get a core temperature of 0.81 keV for buildup time τ_2, and only 140 KJ to get a core temperature 0.93 keV for buildup time τ_3. This is due to the effects of B and $\dot{B}$ on P_m, P_Ω and χ, which were explained in Section 2.1.

9
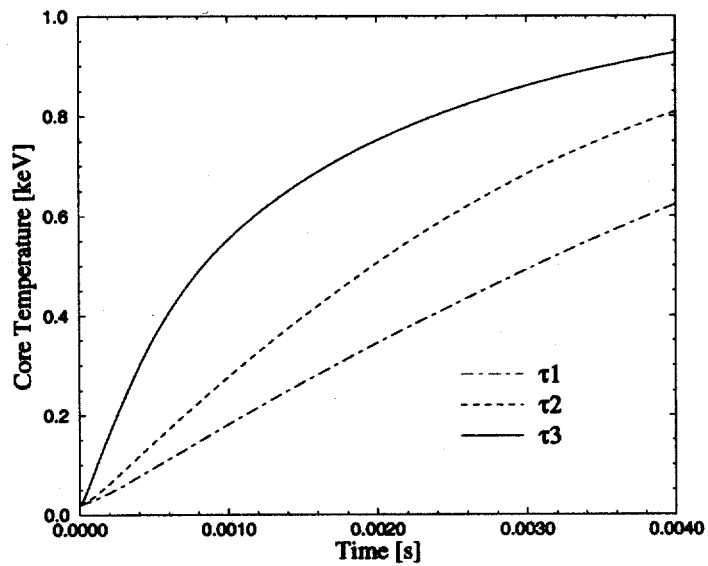
Figure 8: Time evolution of core temperature for τ_1, τ_2 and τ_3.
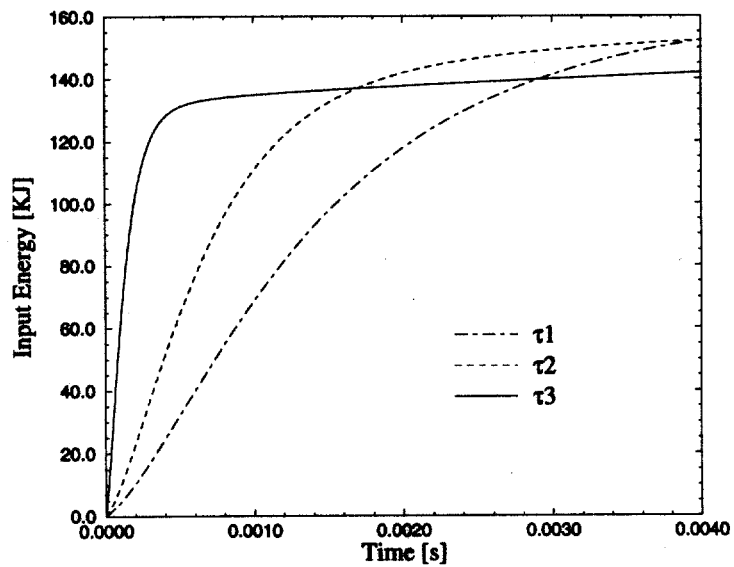

Figure 9: Time evolution of input energy for buildup times τ_1, τ_2 and τ_3.
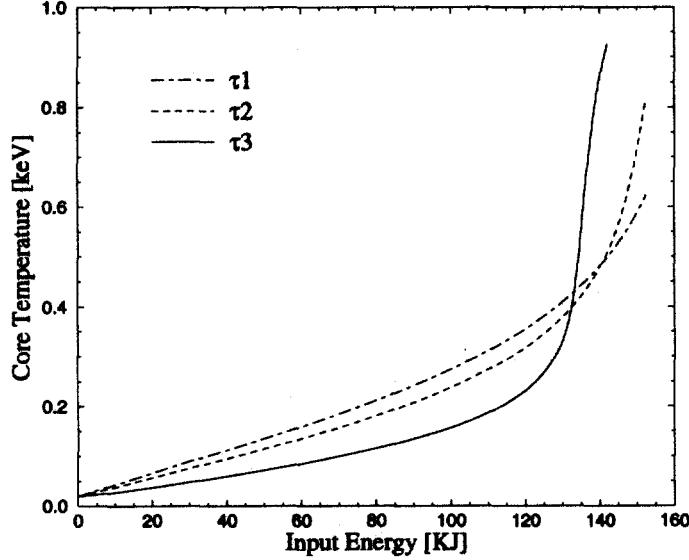
10

Figure 10: Core temperature versus input energy for buildup times τ_1, τ_2 and τ_3.

For example, $T_{c3} < T_{c1}$ from 0 to 133 KJ of total input energy, which corresponds to time intervals $[0, 6.4 \times 10^{-4} \ s]$ for buildup time τ_3 and $[0, 2.6 \times 10^{-3} \ s]$ for buildup time τ_1 from Fig. 9. During those times, (1) the time-averaged $\bar{\chi}_3 = 8500 \ m^2/s$ whereas the time-averaged $\bar{\chi}_1 = 2700 \ m^2/s$ from Fig. 5, and (2) The Ohmic energy input is $\sim 10 \ KJ$ for τ_3 whereas the Ohmic energy $\sim 25 \ KJ$ for τ_1 from Fig. 4. Afterwards, $T_{c3} > T_{c1}$ from 133 KJ onward, which corresponds to time interval $[6.4 \times 10^{-4} \ s, 4 \times 10^{-3} \ s]$ for τ_3, and $[2.6 \times 10^{-3} \ s, 4.0 \times 10^{-3} \ s]$ for τ_1. During those time intervals, (1) the time-averaged $\bar{\chi}_3 = 750 \ m^2/s$ compared to the time-averaged $\bar{\chi}_1 = 960 \ m^2/s$ and (2) the Ohmic energy input is 9 KJ for τ_3 compared to 6 KJ for τ_1. Hence, below $E_{in} = 133 \ KJ$, $\bar{\chi}_3 > \bar{\chi}_1$ and $E_{\Omega 3} < E_{\Omega 1}$ which causes $T_{c3} < T_{c1}$. The situation reverses for $E_{in} > 133 \ KJ$, which causes $T_{c3} > T_{c1}$.

2.4 Other Quantities of Interests

Using Eq. 4, Fig. 11 plots the initial and final ratio of the turbulent magnetic field to the background magnetic field, $\tilde{B}/B = \sqrt{\chi/(v_e L_c)}$. Due to the the decrease in χ (see Fig. 3) and increase in T (hence an increase in v_e), the final ratios are about two orders of magnitude lower than the corresponding initial ratios. Moreover, these ratios have the
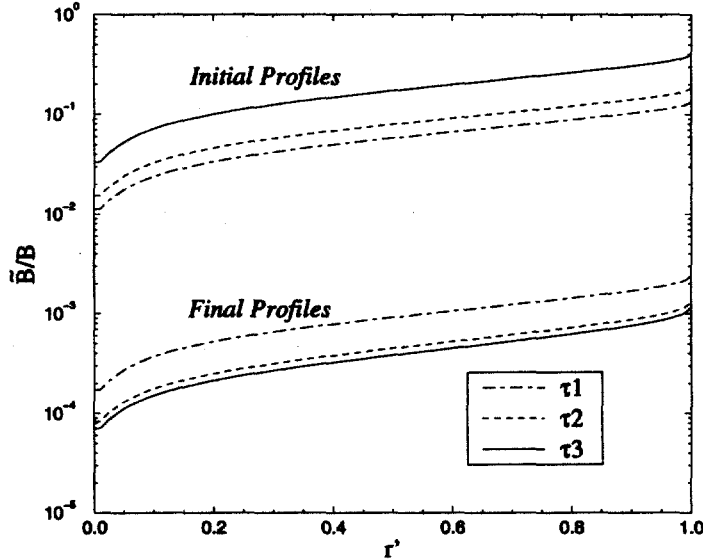
Figure 11: Initial and final $\tilde{B}/B$ for buildup times τ_1, τ_2 and τ_3.

same characteristics as the corresponding diffusion coefficients, shown in Fig. 3: that is, the ratio with buildup time τ_3 is the largest initially and the smallest at the end.

3 Summary

Using corsica's transport module with the thermal diffusivity defined in Eqs. (3) and (4), it takes 140 KJ to heat the electron core temperature from 0.02 keV to 0.93 keV with a magnetic buildup time of $\tau_3 = 1.0 \times 10^{-4}$ s used in Eqs. (7) and (8). The diffusion coefficient for τ_3, the fastest buildup time (among $\tau_1 = 1.0 \times 10^{-3}$ s, $\tau_2 = 5 \times 10^{-4}$ s and $\tau_3 = 1.0 \times 10^{-4}$ s), although initially the largest, rapidly becomes the smallest (on average) due mainly to the rapidly decreasing $\tilde{B}_3$, which decreases the magnetic power P_m and thus decreases the factor g_p in χ_{mag}, which in the regimes of SSPX is the dominant diffusion coefficient.

Of particular interest to the experiment is the issue of optimizing the buildup rate to maximize utilization of the available energy in the electrical systems. Within the present model, if the criterion is reaching high T_c as rapidly as possible, the rapid buildup rate is clearly the most effective. Although the thermal conductivity is very high during the initial

12

buildup, the temperature is low and the thermal energy losses not so fast as to constrain the magnetic field. Then, once the field is developed and its rate of increase reduced, the radial thermal conductivity drops and the temperature increases rapidly. After 4 ms, higher temperatures are reached at lower energy inputs than for the slower buildup rates. Note from Fig. 5 that to the extent that the goal of the experiment is to study low thermal conductivity plasmas, the fastest buildup rate exists in that state much longer than the other two rates modeled.

However, there are effects which lie outside the model and which may require optimization at a slower buildup rate. First, we note from Fig. 11 that at the fastest buildup rate, the initial magnetic field fluctuations in the model exceeds 10%. At this level, the assumption that the configuration is basically one of closed magnetic surfaces with the fluctuations allowing transport without destroying the configuration may not be a good one. Certainly, the possibility that the field is so chaotic that surfaces are not a valid, zeroth-order description must be considered. If so, the entire assumptions of the model need to be re-examined. Furthermore, ion heating by the reconnection process, which has been ignored in the present calculation, is likely to be very strong leading to an energy loss channel which can be significant in an experiment.

A second concern is that wall effects, including impurity generation, may be considerably more serious for the fast buildup; these might become so bad that they prevent the achievement of a high-temperature plasma. Note from Fig. 4 that the magnetic power for the fastest buildup examined is an order-of-magnitude larger than for the slowest. In fact, for the fastest buildup the peak power exceeds 600 MW at its peak, and inefficiencies are not included. This is probably high enough to damage the helicity injector and generate impurities which reach the plasma. The ratios of Ohmic power are closer to a factor of two, so wall heating is not as much greater as magnetic power, but even that factor of two may cause serious wall interactions. This could be locally enhanced by azimuthal asymmetries associated with the large level of magnetic turbulence.

Effects such as these are difficult to model and require experimental study. They indicate the importance of early studies of the effect of buildup rate, and suggest that observation of impurities is important in the confined plasma, the edge plasma, and the gun.

Acknowledgement

References

[1] T. K. Fowler and D. D. Hua, Jour. of Fusion Energy, **14** 181 (1996).

[2] J. B. Taylor, Rev. Mod. Phys. **58**, 741 (1986).

[3] A. B. Rechester and M. N. Rosenbluth, Phys. Rev. Lett. **40**, 38 (1978).

[4] F. J. Wysocki, J. C. Fernandez, I. Henins, T. R. Jarboe and G. J. Marklin, Phys. Rev. Lett. **65**, 40 (1994).

[5] J. A. Crotinger, L. LoDestro, L. D. Pearlstein, A. Tarditi, T. A. Casper and E. B. Hooper, *"Corsica: A Comprehensive Simulation of Toroidal Magnetic-Fusion Devices; Final Report to the LDRD Program."* UCRL-ID-126284, (1997).